

Glass transition in colloidal hard spheres: Measurement and mode-coupling-theory analysis of the coherent intermediate scattering function

W. van Meegen and S. M. Underwood

Department of Applied Physics, Royal Melbourne Institute of Technology, Melbourne, Victoria 3000, Australia

(Received 17 May 1993; revised manuscript received 30 November 1993)

Suspensions of identical particles with hard-sphere-like interactions are studied at concentrations for which the equilibrium state is crystalline. Dynamic light scattering measurements on these suspensions, in their metastable amorphous states prior to crystallization, identify the kinetic glass transition (GT) by the arrest of particle concentration fluctuations on the experimental time scale. This kinetic glass transition coincides with a spectacular change in the mechanism of crystallization from the formation of small crystals, which appear homogeneously nucleated throughout the sample at concentrations below the transition, to the growth, above the transition, of larger and highly asymmetric crystals whose shape and orientation depend on the shear history of the suspension. The intermediate scattering functions are measured over a time window spanning up to eight decades and for several wave vectors near the position of the main structure factor peak. From an analysis of the data in terms of the idealized version of mode-coupling theory, we conclude that both α and β processes are necessary to describe the slow structural relaxation in the fluid near the GT. The superposition principle of the α process, for the colloidal fluid, and the factorization property of the β process, for the colloidal fluid and glass, are verified.

PACS number(s): 64.70.Pf, 61.20.Ne, 82.70.Dd

I. INTRODUCTION

It is now generally accepted that, in principle, all materials are capable of undergoing a glass transition (GT). The basic requirement for vitrification of a fluid is that the rate of cooling or compression must be greater than the intrinsic structural adjustment rate of the liquid [1,2]. While this is readily achieved for network forming glasses, of which window glass is the most familiar example, vitrification of some simple atomic fluids requires cooling rates so large (of order 10^{13} K sec⁻¹) that they can only be attained in computer studies. Lengthening of the structural relaxation time during the temperature or density quench is manifested macroscopically by a corresponding increase in the viscosity of the metastable fluid and the operational GT is generally defined as that temperature or density where the viscosity reaches about 10^{11} Pa s.

The variation of the viscosity with temperature depends on both the material and quench rate. This has led to the proposal of several mechanisms for the GT [1,2]. The description in terms of activated processes with constant energy barriers gives the Arrhenius law which characterizes the exponential viscosity variation with density (or inverse temperature) of so-called strong glass formers. In contrast, kinetic interpretations, where with increasing density the dynamics are viewed in terms of particles being trapped in increasingly persistent neighbor cages, predict an increase in viscosity much sharper than that of the Arrhenius law. The latter behavior is characteristic of fragile glass formers [3].

Although the sudden change in thermodynamic properties, such as the specific heat and thermal expansivity that accompany the freezing in of molecular degrees of freedom at the GT, suggests an underlying second-order phase transition [1,4], a consensus between the thermo-

dynamic and kinetic approaches to the GT remains to be established.

The debate concerning whether and the extent to which the GT is a universal kinetic process has intensified since the application of mode-coupling theory (MCT) to the regime of very dense metastable fluids [5,6]. The main premise of this theory involves nonlinear coupling between pairs of density fluctuations [7,8]. Increasing the strength of this coupling, by decreasing the temperature leads to a dynamic instability where the fluid structure becomes permanently frozen, i.e., a sharp ergodic to nonergodic transition occurs at a critical temperature T_c . The main predictions of the theory are that (i) the approach to the transition, from the fluid, is accompanied by the emergence of two highly nonexponential relaxation processes, the α and β processes, with critically diverging time scales; (ii) arrest of the fluid structure at the transition is signaled by the vanishing of the α process; and (iii) both processes exhibit time scaling properties and, for the β process, fluctuations in space and time are decorrelated.

These predictions apply to the ideal GT. Coupling to current fluctuations to account for phonon-activated hopping motion, the mechanism responsible for the ultimate restoration of ergodicity in molecular glasses, is not included in the basic version of MCT [7,8]. However, even in the best examples of fragile glass formers, such as orthoterphenyl and some mixed ionic fluids, the variation of viscosity with temperature changes from power law to exponential as the GT temperature is approached [9]. The implied change in the underlying mechanism for flow is apparent in computer simulation studies of supercooled atomic fluids. These studies indicate that the nature of the many-particle dynamics changes from that driven by kinetic processes to that dominated by activated trans-

port as the temperature is lowered [10,11]. The critical temperature T_c , obtained from that part of the viscosity versus temperature data which follows a power law, is therefore generally higher than the operational GT temperature. This has led to the suggestion that the basic version of MCT applies only to the moderately supercooled fluid regime (with corresponding viscosities up to about 10 Pa s) [4,5].

Some years ago Pusey and van Meegen showed that a suspension of almost identical submicrometer spherical particles has an equilibrium freezing-melting transition consistent with that expected for the ideal hard-sphere system [12]. They also found that beyond a certain volume fraction ($\phi \sim 0.56$) crystallization was either suppressed or became exceedingly slow [13,14]. At roughly the same concentration structural arrest of the metastable colloidal fluid was indicated by the appearance of a nondecaying component in the intermediate scattering function (ISF). Beyond the initial 10% of the decay, associated with small-scale diffusive particle motions, the ISFs measured at the wave vector corresponding to the peak in the static structure factor were well described by the β process [15]. Subsequent studies of colloidal glasses have yielded quantitative agreement between measured and predicted nonergodicity parameters and verified the factorization property of the β process [16].

Colloidal suspensions offer several advantages over molecular fluids for both fundamental studies of the GT and assessment of the detailed dynamics predicted by MCT. First, the suspensions used in the above work can be regarded as hard spheres in a structureless and incompressible liquid and they therefore constitute the simplest experimental systems to show a GT. Second, the particles exchange energy and momentum only with the suspending liquid so that phonon-activated transport is expected to be suppressed and the observed GT should be illustrative of the ideal GT predicted by the basic version of MCT. This assertion is supported by the ability to describe some eight decades of viscosity variation of colloidal suspensions by power laws [17]. [There is, however, some variation (from $\phi = 0.58$ to 0.71), probably associated with ambiguities in defining the effective hard-sphere volume fraction, in the location of the divergence.] Third, the dynamics of suspensions can be studied by dynamic light scattering (DLS). This technique is ideally suited to explore the structure and dynamics on the spatial scale ($\sim 10^{-7}$ m) and on the temporal scale which ranges from about 10^{-4} sec, for the microscopic diffusive particle motions, to about 10^4 sec, characteristic of the slow structural relaxations near the GT.

This paper goes beyond previous studies [13,14,16] of the GT in suspensions of hard spheres in several respects; (i) we approach the GT in smaller concentration increments, (ii) ISFs are measured over a range of wave vectors that span the static structure factor peak, and (iii) the dynamic window covers over eight decades. Close proximity to the GT and a wide dynamic window are essential if the complete slow relaxation is to be exposed and the crucial scaling predictions of MCT are to be tested. As outlined in a previous Letter [18], our results

show unequivocally that, in the metastable fluid close to the GT, relaxation beyond the time scale of the microscopic diffusive motion proceeds in two stages. Significantly, we demonstrate that these slow relaxation stages can only be fully described by a combination of both α and β processes.

Further to Ref. [18] we present several important consistency checks of the quantities obtained by a MCT analysis of our data. These show that the basic version of MCT describes the relaxation processes outside the microscopic transients, on suspensions at concentrations in the vicinity of the GT, to an accuracy of 10–20 % using effectively a single fitting parameter. We also pay particular attention to the procedures for acquiring reliable ISFs close to the GT where the time scales of the slowest fluctuations are comparable to the experimental time. These more detailed studies allow us to confirm the existence of a mechanism, other than “hopping,” that is responsible for the very slow crystallization of colloidal glasses.

In the following section of this paper we give an outline of the MCT predictions essential for analysis of the experimental results. Experimental methods, encompassing a description of the samples and a discussion of the light scattering procedures, are given in Sec. III. Section IV contains a presentation and discussion of the results; this includes DLS results, a discussion which attempts to reconcile the particle dynamics in the metastable colloidal fluids and glasses with observed crystallization processes, and analysis of the DLS data in terms of MCT. Concluding remarks are presented in Sec. V.

II. THEORY

An outline of dynamic light scattering theory is given in Sec. III B along with a verification of the experimental procedures appropriate to different suspension concentration regimes. Here we give an exiguous account of mode-coupling theory, concentrating on those aspects necessary for an interpretation of the DLS results. Two recent reviews [7,8] give a comprehensive description of MCT and appraise a large body of experimental data.

Since the dynamics of colloidal suspensions are diffusive on all relevant time scales, we start with the following formally exact memory equation for the normalized intermediate scattering function (or autocorrelation function of number density fluctuations) $f(q, \tau)$:

$$\dot{f}(q, \tau) + \omega(q) \left[f(q, \tau) - \int_0^\tau H(q, \tau-s) f(q, s) ds \right] = 0, \quad (1)$$

where $\omega(q) = D_0 q^2 / S(q)$ is the frequency associated with the smallest scale particle diffusion, D_0 is the free particle diffusion coefficient, and $S(q)$ is the static structure factor. Equation (1) may be obtained from the Smoluchowski equation by using standard projection operator procedures [19]. Laplace transformation gives the formal solution

$$f(q, z) = \{z + \omega(q)[1 - H(q, z)]\}^{-1}. \quad (2)$$

Cichocki and Hess [20] have shown that the memory function $H(q, z)$ can be expressed in terms of an irreduc-

ible memory function $M(q, z)$ as follows:

$$H(q, z) = M(q, z) / [1 + M(q, z)] . \quad (3)$$

It is then assumed that the function $M(q, z)$ can be written as [7,8,21]

$$M(q, z) = \nu(q) + \omega(q)m(q, z) , \quad (4)$$

where $\nu(q)$ is a white noise term. Combining Eqs. (2)–(4) gives

$$f(q, z) / [1 - zf(q, z)] = [1 + \nu(q) + \omega(q)m(q, z)] / \omega(q) . \quad (5)$$

The form for the memory kernel, or random force correlator $m(q, \tau)$, which predicts at least the main qualitative dynamical features observed around the GT is [7,8]

$$m(q, \tau) = \sum_{q', q''} V(q; q', q'') f(q', \tau) f(q'', \tau) . \quad (6)$$

The vertices $V(q; q', q'')$ depend only on the static structure factor $S(q)$. While the choice of $m(q, \tau)$ is uncontrolled, one arrives at Eq. (6) with the argument that fluctuations in the random force should decay into pairs of number density fluctuations and the approximation that the average of products of density fluctuations factorizes into products of averages [7,22].

On smoothly changing $S(q)$, corresponding to increasing the volume fraction ϕ (or reducing temperature in molecular glass formers), the solution to these equations shows a dynamic instability at a critical concentration ϕ_c ; for $\phi < \phi_c$, $f(q, \tau)$ decays to zero, while for $\phi > \phi_c$, $f(q, \tau)$ saturates in time to a finite positive value $f(q, \infty)$. Physically, this instability has the signature of an ideal GT, a transition from ergodic to nonergodic behavior. It must be emphasized that the system does not exhibit any anomaly in $S(q)$ as this instability is traversed.

Close to the GT and small z (i.e., long times) the memory function becomes large and Eq. (5) reduces to

$$f(q, z) / [1 - zf(q, z)] = m(q, z) , \quad (7)$$

i.e., the slow dynamics near the GT do not depend explicitly on the microscopic dynamics characterized by the quantities $\nu(q)$ and $\omega(q)$. Solutions in this asymptotic regime, valid to order $|\sigma|^{1/2}$ in the separation parameter

$$\sigma = c_0(\phi - \phi_c) / \phi_c , \quad (8)$$

where c_0 is a material-dependent constant, have been extensively studied [7,8] and, from an experimental standpoint, are most interesting and challenging.

Here the theory predicts that beyond the time scale t_0 [$\sim (\omega^{-1}(q))$] of the microscopic motions the relaxation of $f(q, \tau)$ proceeds in two stages. These stages are characterized by two time scales τ_α and τ_β , which diverge as the separation parameter approaches zero:

$$\tau_\alpha = t_0 |\sigma|^{-\gamma} , \quad \gamma = (1/2a) + (1/2b) , \quad (9a)$$

$$\tau_\beta = t_0 |\sigma|^{-\delta} , \quad \delta = 1/2a . \quad (9b)$$

The nonuniversal exponents a ($0 < a < 0.5$) and b ($0 < b < 1$) are related to the exponent parameter λ as fol-

lows:

$$\lambda = \Gamma^2(1-a) / \Gamma(1-2a) = \Gamma^2(1+b) / \Gamma(1+2b) , \quad (10)$$

where Γ is the gamma function. The dynamics during the first of these slow relaxation stages, in the time regime $t_0 \ll \tau \ll \tau_\alpha$, are governed by the β process where

$$f(q, \tau) = f_c(q) + |\sigma|^{1/2} h(q) g_\pm(\tau / \tau_\beta) . \quad (11)$$

Here $f_c(q)$ is the nonergodicity parameter and represents the amplitude of the arrested structure at ϕ_c . $f_c(q)$ as well as the critical amplitude $h(q)$ and the universal master function $g_\pm(\tau)$ (where the subscript \pm denotes the sign of σ) are independent of concentration. Concentration enters the dynamics only through the parameter σ and the scaling times τ_α and τ_β [Eq. (9)]. The factorization of the spatial and temporal variables, indicated in Eq. (11), suggests that localized dynamics promote relaxation of concentration fluctuations to the value $f_c(q)$. On the fluid side of the transition ($\sigma < 0$) the time τ_β marks the crossover to the second relaxation stage, the α process, which describes relaxation of $f(q, \tau)$ to zero. For this process another scaling law, valid for $\tau \gg \tau_\beta$, is predicted,

$$f(q, \tau) = f_c(q) G(q, \tau / \tau_\alpha) . \quad (12)$$

The nonuniversal functions $G(q, \tau)$ are independent of concentration. In the glass ($\sigma > 0$) the α process is arrested but the β process persists and saturates at long times to the value $g_+(\tau \rightarrow \infty) = (1-\lambda)^{-1/2}$.

We state two limiting results:

$$g_\pm(\tau \ll \tau_\beta) = (\tau / \tau_\beta)^{-a} , \quad (13)$$

$$g_-(\tau_\beta \ll \tau \ll \tau_\alpha) = -B(\tau / \tau_\beta)^b , \quad (14)$$

where $B > 0$.

These predictions may be given the following physical interpretation [8]. The β process describes the dynamics of localized particle clusters or cages and Eq. (13) indicates that during the early part of this process the dynamics in the fluid ($\sigma < 0$) and glass ($\sigma > 0$) are indistinguishable; the algebraic form reflects the fractal nature of the lifetimes of these metastable clusters. The α process describes the breakdown of the particle cages leading to large-scale particle diffusion and flow. The dynamics of the particle cages on the verge of breaking up is shared by both α and β processes and is described by the von Schweidler law, Eq. (14).

Equation (7) can be obtained from either the Liouville equation [8] or, as outlined above, the Smoluchowski equation [21]. Thus the GT scenario, embodied in Eqs. (9)–(14), applies both to systems where the microscopic dynamics is ballistic and to those where it is diffusive. The material specific potential-energy function enters only via the static structure factor. In particular, $S(q)$ determines the exponent parameter λ which in turn specifies $g_\pm(\tau)$ and the other exponents through Eq. (10). The connection between the time scales of the predicted functions and the microscopic transients is made in Eq. (9) with the time t_0 ; the latter is in principle the only presently undetermined parameter in the theory.

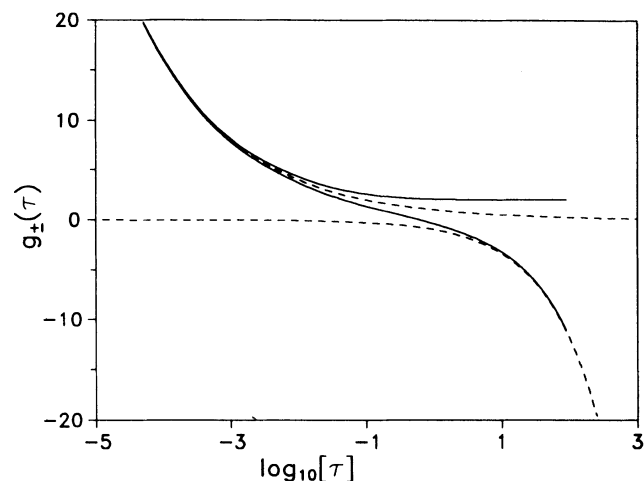


FIG. 1. Universal master functions of the β process for the hard-sphere system (drawn for $\lambda=0.758$). The upper and lower solid curves are the functions $g_+(\tau)$ and $g_-(\tau)$, respectively. The upper and lower dashed curves are the critical decay τ^{-a} [Eq. (13)] and the von Schweidler law $-B\tau^b$ [Eq. (14)].

Mode-coupling theories for the GT have not yet taken into account the hydrodynamic interactions which, in concentrated suspensions, couple the diffusive particle motions to the structure [23]. However, previous analyses [15] have found the concentration dependence of t_0 to be small in comparison with that of τ_α and τ_β , indicating that, at suspension concentrations near the GT, the slowing of structural relaxation is strongly dominated by the cage effect.

In comparing the dynamics of molecular glass formers such as polymers and ionic systems with MCT, λ is treated as a free parameter [8,24]. For the hard-sphere system reasonably accurate approximations for $S(q)$ are available for volume fractions up to freezing [25]. Extending these approximations into the metastable fluid region has allowed the evaluation of the exponents and the functions

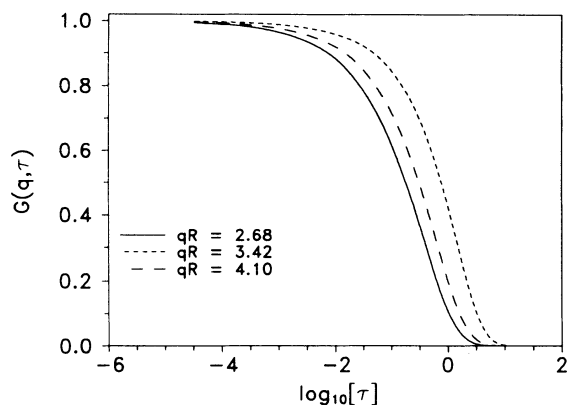


FIG. 2. Master functions of the α process shown for the wave vectors indicated. R is the effective hard-sphere particle radius. The location q_m of the main peak of the static structure factor (see Fig. 8) for the hard-sphere fluid at freezing is given by $q_m R = 3.46$.

appearing in Eqs. (9)–(14); in particular, $\phi_c = 0.525$, $a = 0.301$, $b = 0.545$, $\lambda = 0.758$, and $B = 0.963$ [26–28]. c_0 depends sensitively on $S(q)$ and the value $c_0 = 1.2$ or 1.4 is obtained for the Verlet-Weis or Percus-Yevick approximations, respectively [29]. The universal master functions $g_\pm(\tau)$ of the β process are shown in Fig. 1 and the q -dependent master functions $G(q, \tau)$ of the α process are shown in Fig. 2 for three of the wave vectors for which the ISFs have been measured.

This constitutes the basic version of MCT in which a sharp transition from a fluid to an ideal glass is predicted. Inclusion of particle current relaxations in the memory kernel $M(q, \tau)$, to allow for possible activated transport, smears the sharp transition [30,31]. However, since the motions of colloidal particles in a fluid are strongly overdamped, it is improbable that a particle can acquire enough energy to hop over barriers in the free energy landscape. We expect, therefore, the basic version of MCT to be applicable to colloidal suspensions.

III. EXPERIMENTAL DETAILS

A. Description of colloidal suspensions

The preparation and characterization of suspensions used here have been described in detail in previous papers [14,16]. Briefly, these suspensions contain poly(methylmethacrylate) particles, stabilized against irreversible aggregation by thin (~ 10 nm) steric barriers of poly-(12-hydroxystearic acid). The hydrodynamic radius $R_H = 205 \pm 3$ nm and polydispersity ($\sim 4\%$) of the particles were determined by DLS on very dilute samples [32]. For the concentrated suspensions the composition of the suspending liquid, a mixture of decalin and carbon disulfide, was adjusted until the turbidity was about 0.2 cm^{-1} . Thus the samples, prepared in optical cuvettes of 1-cm^2 cross section, appeared almost transparent and the light scattering analysis (discussed below) assumes the validity of the first Born approximation.

The equilibrium phase behavior of these suspensions mimics that of the ideal hard-sphere system [12,33,34]. Exploitation of this property allows expression of the suspension concentrations in terms of effective hard-sphere volume fractions $\phi = \xi \phi_f / \xi_f$, where ξ is the “core” volume fraction (calculated from the weight composition of the samples and literature values of the densities of the components), ξ_f the measured core volume fraction where the colloidal fluid freezes, and $\phi_f = 0.494$ the volume fraction at which the perfect hard-sphere fluid freezes [35]. The difference between freezing and melting concentrations is sensitive to deviations from a hard-sphere pair interaction [36]. It is therefore significant that the experimental melting volume fraction $\phi_m = 0.542 \pm 0.003$ is in agreement with the value 0.545 ± 0.002 established by computer simulation for the hard-sphere crystal [35]. On the basis of this agreement we regard these suspended particles as hard spheres.

The particles are easily redispersed or randomized from either a gravitationally compacted sediment or a crystalline state by tumbling the samples on a vertical wheel rotating at about 1 Hz. The amorphous appear-

ance of the samples and the fluidlike form of their static structure factors, measured following this tumbling process [14], suggest that suspensions at $\phi > \phi_f$ are in a metastable fluid state. In this sense the process of concentrating a suspension to a value $\phi > \phi_f$ followed by tumbling can be regarded as analogous to a density quench of a hard-sphere fluid.

When left undisturbed following this quench, the suspensions crystallize. The volume fractions of the samples studied here and the times T_x when Bragg reflecting crystals first become evident are listed in Table I. Detailed descriptions of the observed crystallization have been presented elsewhere [12,34,37]. The main features shown by the suspensions used in this study are as follows: For samples whose concentrations lie between the freezing and melting concentrations, gravity separates an increasing proportion of coexisting polycrystalline phase (at volume fraction ϕ_m) from the fluid phase (at ϕ_f). Beyond melting progressively smaller crystals, roughly isometric and nucleated at randomly distributed sites, grow and occupy the entire sample volume. These small crystals are barely visible to the naked eye at $\phi=0.574$. (Crystal growth in this sample was observed more quantitatively by the development of a diffraction broadened Bragg peak [14].) Remarkably, the sample for which the concentration is only 1% higher ($\phi=0.581$) develops much larger and highly asymmetric crystals (average largest dimension of about 1 mm). We also draw attention to the considerable increase in the crystallization time (Table I, see also Ref. [38]) that accompanies this small increase in concentration.

It appears, therefore, that at some concentration ϕ_g ($0.574 < \phi_g < 0.581$) there is a change in the crystallization mechanism from homogeneous nucleation and growth to a much slower crystal growth on highly asymmetric, plate-shaped nuclei [37]. We tentatively identify ϕ_g as the GT concentration. In Sec. IV A we attempt to reconcile these observations with the particle dynamics measured by DLS on the metastable fluids.

Apart from those samples with volume fractions close

to the melting point ($0.540 < \phi < 0.555$), where the combination of thermodynamic drive and kinetic mobility apparently provide optimum conditions for crystal nucleation and growth, T_x was considered to be sufficiently long to make meaningful DLS measurements on the metastable fluids.

B. Dynamic light scattering

The optical arrangement and other details relevant to dynamic light scattering experiments on colloidal fluids and glasses have been described in previous papers [14,16]; only an outline is given here. However, we address in some detail the procedures employed to obtain reliable estimates of the intermediate scattering functions close to the GT, where the time scales of the slowest relaxation processes are comparable with the duration of a single measurement.

In DLS one measures the time-averaged time correlation function

$$g_T^{(2)}(q, \tau) = \langle I(q, 0), I(q, \tau) \rangle_T / \langle I(q) \rangle_T^2 \quad (15)$$

of the scattered intensity $I(q, t)$. The magnitude of the wave vector \mathbf{q} is $q = (4\pi n / \lambda_0) \sin(\theta/2)$, where λ_0 is the vacuum wavelength of the radiation, n the refractive index of the medium, and θ the scattering angle. In the conventional operation of DLS [39,40] it is tacitly assumed that, in the course of an experiment of some reasonable duration T , the N particles in the system (or scattering volume V) access at least a representative fraction of the full ensemble of spatial configurations, i.e., the system is ergodic, so that the time average, denoted by the brackets $\langle \rangle_T$ in Eq. (15), is equivalent to the ensemble average $\langle \rangle_E$. We express this property by

$$g_T^{(2)}(q, \tau) = g_E^{(2)}(q, \tau) . \quad (16)$$

A consequence of a system's ergodicity is that the amplitude of the field scattered to a point in the far field

$$E(q, t) = \sum_{j=1}^N \exp[i\mathbf{q} \cdot \mathbf{r}_j(t)] \quad (17)$$

TABLE I. Sample concentrations expressed as effective hard-sphere volume fractions ϕ , sample designation, crystallization time T_x , duration of a single DLS measurement T (in seconds), coherence factor c , number of measurements M between tumbling of the samples, total number of measurements K , and procedure (as discussed in Sec. III B) used to determine $f(q, \tau)$ from $g_T^{(2)}(q, \tau)$.

ϕ	Designation	T_x	T (sec)	c	M	K	Procedure
0.494	F2	NA	1000	0.98	5	5	(i)
0.528	F6	30 min	500	0.98	3	6	(i)
0.535	H9	12 min	500	0.20	1	10	(i)
0.542	H10	< 10 min					
0.546	H11	< 10 min					
0.551	H1	< 10 min					
0.558	H3	20 min	500	0.20	1	10	(ii)
0.567	H5	100 min	1000	0.20	4	40	(ii)
0.574	H6	120 min	1000	0.20	4	40	(ii)
0.581	H7	6 h	1000	0.20	15	180	(ii)
				0.98	15	15	(iii)
0.587	H8	10 h	1000	0.20	15	180	(ii)
				0.98	15	15	(iii)

is a complex Gaussian random variable with zero mean. Here $E(q, t)$ applies to N identical spherical particles located at $\mathbf{r}_j(t)$ in an optically homogeneous background. (Possible effects of the small spread in the particle size distribution are discussed below. The particle scattering amplitude has been omitted because it cancels through normalization.) $E(q, t)$ represents the spatial Fourier component, of wave vector \mathbf{q} , of particle concentration fluctuations

$$E(q, t) = \delta\rho(q, t) = \int \delta\rho(\mathbf{r}, t) \exp[i\mathbf{q} \cdot \mathbf{r}(t)] d\mathbf{r}. \quad (18)$$

The normalized (ensemble-averaged) autocorrelation function of the scattered light field or ISF, $f(q, \tau)$, the central quantity of interest, is related to $g_E^{(2)}(q, \tau)$ by the standard Siegert relationship [40]

$$g_E^{(2)}(q, \tau) = 1 + c [f(q, \tau)]^2, \quad (19)$$

where c , the coherence factor, is determined by the ratio of the coherence area (or speckle size) to the detector area. The ISF is given by

$$f(q, \tau) = F(q, \tau) / F(q, 0), \quad (20)$$

where

$$F(q, \tau) = \langle E(q, 0) E^*(q, \tau) \rangle_E \quad (21)$$

and $F(q, 0) = S(q)$ is the static structure factor. In view of Eq. (18) the ISF, $f(q, \tau)$, represents the normalized autocorrelation function of particle concentration fluctuations.

For metastable colloidal fluids at concentrations approaching the GT, the time scale τ_r of the slowest structural relaxations diverges. In principle the duration T of the measurement could be increased so as to capture a representative sample of these slow fluctuations provided that there is no macroscopic change in the system during the measurement. However, since the objective here is to study the particle dynamics in the metastable colloidal fluid, the maximum duration of a single measurement is limited, at least, by the crystallization time T_x . We therefore proceeded as follows: First, the scattering volume was enlarged, by using an unfocused laser beam and an increased detector aperture, to give a coherence factor of $c = 0.2$. With this arrangement the detector accepts about five coherence areas of the scattered light field, corresponding to five independent spatial Fourier components of the particle concentration fluctuations. Second, for every sample a total of K measurements were made each of duration T (which in most cases was 1000 sec); a sample was tumbled every M ($M < K$) measurements. In addition, between each measurement the sample was moved relative to the laser beam so that a different region was illuminated. To be confident that the measurements applied to the metastable fluid and that they were not affected by crystallization, both T and M were limited to ensure, first, that $MT < T_x$ and, second, that there was no systematic variation over the M data sets obtained after tumbling the samples. The measurement duration T and numbers M and K are listed in Table I.

From the K measurements of the (unnormalized) time-averaged intensity correlation function $\langle I(q, 0) I(q, \tau) \rangle_T^{(j)}$ and the time-averaged intensity $\langle I(q) \rangle_T^{(j)}$ ($j = 1, K$) estimates of the (normalized) ensemble-averaged intensity autocorrelation function were obtained from

$$g_{E(m)}^{(2)}(q, \tau) = \frac{\sum_{j=1}^m \langle I(q, 0) I(q, \tau) \rangle_T^{(j)}}{\left[\sum_{j=1}^m \langle I(q) \rangle_T^{(j)} \right]^2}. \quad (22)$$

ISFs were then calculated by using Eq. (19) from the average of the K/m estimates of $g_{E(m)}^{(2)}(q, \tau)$. Clearly as $m \rightarrow \infty$, $g_{E(m)}^{(2)}(q, \tau) = g_E^{(2)}(q, \tau)$. However, one sees from Fig. 3(a), where estimates of $f(q, \tau)$ based on $g_{E(m)}^{(2)}(q, \tau)$ for $m = 1, 4, 10$, and 40 are shown for the most concentrated sample below the GT ($\phi = 0.574$), that provided $m \geq 10$ we obtain results free from distortions which may occur as a result of inadequate sampling over the slowest fluctuations. Thus, at this concentration a combination of time averaging (over 1000 sec) and ensemble averaging (over about $m/c = 50$ independent spatial Fourier components) is required to capture a statistically significant

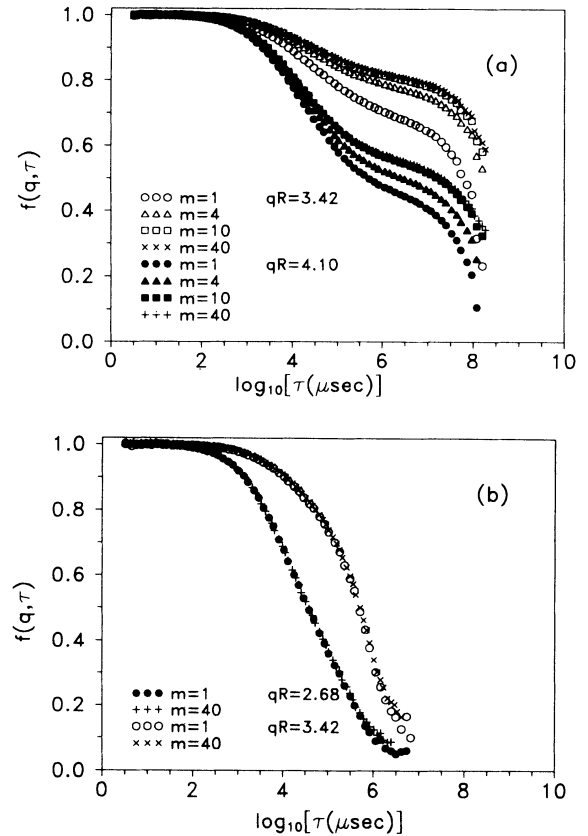


FIG. 3. Intermediate scattering functions versus the logarithm of the delay time τ for (a) $\phi = 0.574$ and (b) $\phi = 0.535$ estimated from Eqs. (16) and (22) using different numbers m of independent measurements of time-averaged intensities and intensity autocorrelation functions. See Sec. III B for details. The ISF's shown here and in subsequent figures are normalized so that $f(q, 0) = 1$.

sample of the slowest relaxation processes whose time scales are of order 1000 sec. However, at the lower concentration, $\phi=0.535$, the fact that the estimated $f(q,\tau)$ is independent of $m (\geq 1)$ indicates that $\tau_r \ll 1000$ sec [Fig. 3(b)].

For the nonergodic glass phase Pusey and van Megen [41] have proposed a model which leads to a procedure for estimating the ISF from the measured time-averaged intensity autocorrelation function that is more straightforward than that just described for very concentrated metastable fluids. The model assumes that the particles are able to execute only restricted (Brownian) excursions about an amorphous distribution of fixed average positions and that correlations in these excursions decay to zero in the course of a measurement. The relationship between the ISF and the measured time-averaged intensity autocorrelation function $g_T^{(2)}(q,\tau)$ is [41-43]

$$f(q,\tau) = 1 + (I_T/I_E) \{ [g_T^{(2)}(q,\tau) - g_T^{(2)}(q,0) + 1]^{1/2} - 1 \}. \quad (23)$$

$I_T = \langle I(q) \rangle_T$ is the time-averaged intensity and is given by the average number of photon detections accumulated during a particular measurement. $I_E = \langle I(q) \rangle_E$ is the ensemble-averaged intensity and, as described in Ref. [16], may be determined from the photon counts accumulated while the sample is moved gently at constant speed in the laser beam. Equation (23) applies only for a point detector, i.e., the coherence factor $c = 1$. This requirement is achieved in practice by making the detector area much smaller than one coherence area.

To recapitulate, the relaxation time τ_r of the slowest structural relaxations relative to the measurement time T determines which of the following three procedures is most appropriate for estimating the ISFs of metastable colloidal fluids and glasses.

(i) $T \gg \tau_r$: The experimental duration significantly exceeds the time scale of the slowest concentration fluctuations. There is no doubt about the system's ergodicity, Eq. (16) applies, and $f(q,\tau)$ can be calculated from a single measurement of the time-averaged intensity autocorrelation function with Eq. (19).

(ii) $T \sim \tau_r$: The time scale of the slowest fluctuations in the suspension is comparable with the experimental time. In these cases the ensemble-averaged intensity autocorrelation function $g_E^{(2)}(q,\tau)$ is estimated from the sum of m independent measurements of the mean intensities and (unnormalized) intensity correlation functions [Eq. (22)]. Equation (19) is then employed to determine $f(q,\tau)$.

(iii) $T \ll \tau_r$: Part of the concentration fluctuations is effectively arrested on the experimental time scale and $f(q,\tau)$ is calculated from a single measurement of the time-averaged intensity autocorrelation function $g_T^{(2)}(q,\tau)$ and the ensemble-averaged intensity $\langle I(q) \rangle_E$ with the use of Eq. (23).

Although we have recently given an extensive verification of Eq. (23) for colloidal glasses [16,42], one might still question its validity very close to the GT; at what stage (or suspension concentration) does τ_r become so large (relative to T) that it can be regarded as infinite? We address this issue in Fig. 4 where we compare esti-

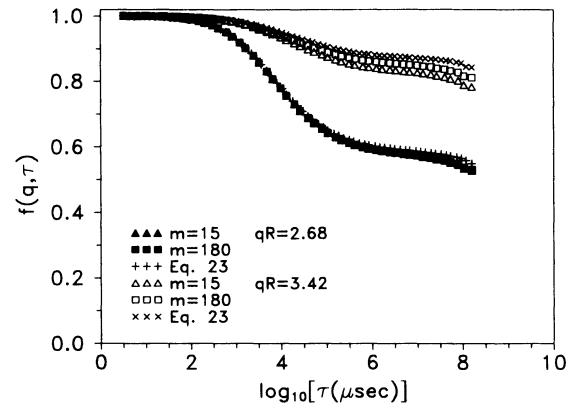


FIG. 4. Intermediate scattering functions for the lowest concentration glass $\phi=0.581$. Estimates obtained by the "brute-force" procedure (ii) are shown by the triangles and squares based on the indicated m independent measurements of the time-averaged intensities and intensity autocorrelation functions. Estimates based on Eq. (23) are shown by the crosses and plus signs.

mates of $f(q,\tau)$ obtained by procedures (ii) and (iii) for our lowest concentration colloidal glass (the first sample in which homogeneously nucleated crystallization is suppressed). Note first that for $\tau \gtrsim 10^6 \mu\text{sec}$ $f(q,\tau)$ saturates to an almost constant value. We discuss this structural arrest fully in Sec. IV and, for now, only mention that the q dependence of the amplitude of the arrested structure in the glass phase, indicated by the long-time plateau value of $f(q,\tau)$, varies in harmony with the static structure factor $S(q)$ [16,26]. The feature in Fig. 4, pertinent to the present discussion, is that as we increase the number (m/c) of independent spatial Fourier components used in procedure (ii), the estimate of the ISF converges to that obtained by procedure (iii). Below the position q_m of the peak in $S(q)$, where about 50% of the concentration fluctuations is arrested [$f_c(qR=2.68) \sim 0.5$; see Sec. IV C], it appears that about 75 ($m=15$ and $c=0.2$) independent spatial Fourier components are sufficient to obtain a reasonable estimate of the ensemble average over the arrested structure. However, near q_m , where $f_c(qR=3.42) \sim 0.8$, it appears that more than 900 independent spatial Fourier components are required to cover the ensemble of this Fourier component ($q \sim q_m$) of the concentration variations. [A quantitative statistical analysis of this "brute-force" procedure (ii) will be the subject of a future publication [44].] We therefore conclude that even for the lowest concentration colloidal glass in this study ($\phi=0.581$) the less tedious procedure (iii) leads to reliable estimates of $f(q,\tau)$.

IV. RESULTS AND DISCUSSION

A. Light scattering results

As mentioned in Sec. III A, except near the melting concentration $\phi_m=0.545$, crystallization of the suspensions after tumbling was sufficiently slow (see Table I) to

permit reproducible DLS measurements in the metastable fluid phases. The coexisting equilibrium fluid phase at freezing ($\phi_f=0.494$) plus seven metastable colloidal fluids, spanning a concentration range from $\phi=0.528$ to 0.587 , were studied at several wave vectors in the region of the position q_m of the primary peak of the static structure factor. The procedures used to estimate the ISF from the measured time-average time correlation functions are listed for each sample in Table I.

Our basic results for the ISFs are shown in Fig. 5 for three different wave vectors; complimentary results at other wave vectors are shown in Fig. 1 of Ref. [18]. The wave vectors are expressed in dimensionless form as qR , where $R = 199$ nm is the effective hard-sphere particle radius, obtained by matching the positions of the structure factor peaks of the colloidal suspension and ideal hard-sphere fluid at their respective freezing concentrations [14,16]. If we define, for the purpose of a qualitative discussion, the overall decay time of the ISF as that where $f(q,\tau)=0.5$, one sees from Fig. 5(b), for example, that an increase in suspension concentration from very dilute ($\phi\sim 0$) to the freezing concentration ($\phi_f=0.494$) is accompanied by a lengthening of the overall decay time by slightly less than two decades, from about 10^3 to 10^5 μsec . Increasing the concentration further, from ϕ_f to $\phi=0.574$, incurs an increase in decay time by another four decades, from about 10^5 to 10^9 μsec , and three relaxation stages become apparent.

The decay of correlations of concentration fluctuations associated with the smallest scale diffusive motion is given by $\exp[-D(q)q^2\tau]$; $D(q)$ is the wave-vector-dependent short-time diffusion coefficient obtained from the initial slope of $f(q,\tau)$ [23,45]. To prevent overcrowding of the figures the quantity $\exp[-D(q)q^2\tau]$ for the freezing concentration is only included in Fig. 5(b). It appears, however, that this small-scale diffusive motion accounts for approximately the first 5% of the total decay of $f(q,\tau)$ and extends to just below 10^4 μsec . The following two relaxation stages are most clearly delineated for $\phi=0.574$ where an inflection point, in $f(q,\tau)$ versus τ , at $\tau\sim 10^4$ μsec suggests a crossover from relaxation associated with the microscopic motions to a second relaxation process. Another inflection at $\tau\sim 10^7$ μsec points to a second crossover to a third process. Interestingly, these crossover times appear to be independent of the wave vector. At lower concentrations the two slow relaxation processes merge and contract to shorter times.

For the volume fraction $\phi=0.574$ the slow but pronounced downward curvature of $f(q,\tau)$ at long times implies that the time scale of the slowest concentration fluctuations is comparable to the duration ($T=1000$ sec) of the measurement. (We came to a similar conclusion for this sample in Sec. III B.) However, when the concentration is increased by merely 1%, from 0.574 to 0.581 , $f(q,\tau)$ approaches an almost constant value at long times. Thus at $\phi=0.581$ the time scale of the slowest fluctuations lengthen to the extent that they are effectively arrested during the course of a single measurement.

The above observations indicate the occurrence of a kinetic GT at a concentration ϕ_c ($0.574 < \phi_c < 0.581$).

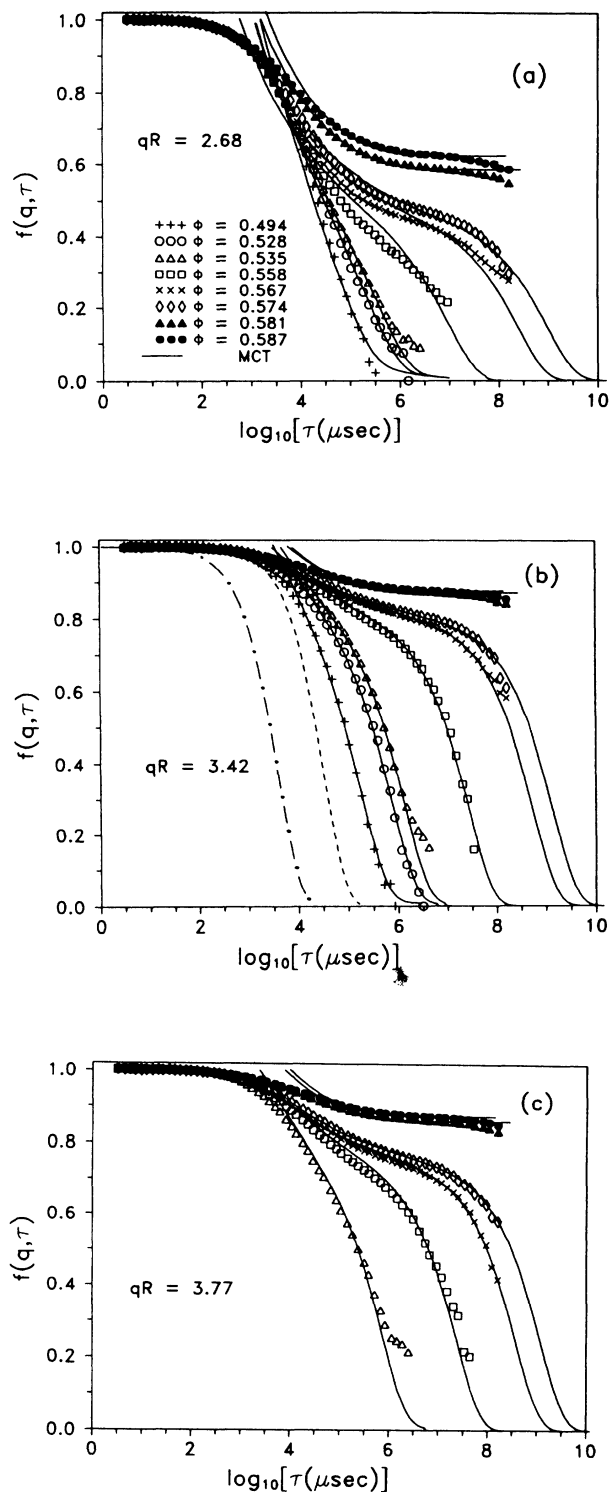


FIG. 5. Intermediate scattering functions for three wave vectors [(a)–(c)] around the structure factor peak. The symbols refer to the experimental data for suspension volume fractions indicated in (a). The solid curves are the MCT fits to the data, as discussed in Sec. IV C. The additional curves in (b) are $\exp[-D_0q^2\tau]$ (---) and $\exp[-D(q)q^2\tau]$ (-.-.-), where D_0 is the free particle diffusion coefficient and $D(q)$ is the short-time collective diffusion coefficient for the colloidal fluid at freezing ($\phi=\phi_f$) at $qR=3.42$.

Here large-scale diffusion ceases and the fluid structure, at all wave vectors, becomes effectively frozen.

B. Crystallization and the glass transition

The arrest of concentration fluctuations in the metastable colloidal fluid coincides with the spectacular change of the crystallization mechanism, described in Sec. III A, in these suspensions when they are left undisturbed for long periods after tumbling [37]. The concentration ϕ_g , where homogeneously nucleated crystallization becomes suppressed, coincides with the value ϕ_c , where a fraction, indicated by the long-time limiting values of $f(q, \tau)$ in Fig. 5, of the concentration fluctuations is arrested. These observations suggest that homogeneous nucleation demands the kinetic assistance of full structural relaxation, i.e., large-scale particle diffusion.

In previous work [16] we speculated that the large irregular crystals observed throughout the bulk suspensions at concentrations just greater than ϕ_g were grown epitaxially on traces of contaminants. We also suggested that, for $\phi > \phi_c$, the small remnant decay of the ISFs at long times was associated with the small ($\sim 4\%$) spread in the particle size distribution and a trace concentration of very small but mobile particles with the freedom to roam in the predominantly arrested structure of average-sized particles. As a result of this more detailed study we now offer an alternative explanation which reconciles the slight reduction of $f(q, \tau)$ at long times ($\tau > 10^6 \mu\text{sec}$) with the nucleation and slow growth of irregular crystals.

We suggest that these highly asymmetric and large crystals grow on plate or needle shaped nuclei that are shear induced by the tumbling procedure used to randomize the particle positions. (These shear-induced microstructures parallel to the flow direction have been revealed by the appearance of isolated intensity maxima in light diffraction studies of suspensions in Couette flow [46]. Their formation is also manifested by a reduction in the shear viscosity [17].) This explanation is supported by the observation that the size, shape, and orientation of the crystals, which develop at suspension concentrations in excess of ϕ_g , depend on the shear history, for example, slow tumbling on the vertical wheel, sonication, or subjecting the sample to a small-amplitude regular rocking motion of several hertz. After tumbling the sample at $\phi_g = 0.587$, for instance, seemingly randomly orientated crystals, with a largest average dimension of about 3 mm, become evident after about 24 h, whereas much smaller needle-shaped crystals, mostly parallel to the cuvette walls, develop within minutes of commencing a regular rocking motion [37].

It is possible, by means of the rocking motion, to induce needle-shaped crystals in all suspensions at concentrations larger than 0.550. Presumably, at lower concentrations the structural relaxation rate is greater than the local shear rate. On leaving samples with concentrations in the range $0.55 < \phi < \phi_g$ undisturbed the shear-induced crystals mostly dissipate and are eventually replaced by the more symmetric homogeneously nucleated crystals. However, for $\phi > \phi_g$, the needle-shaped crystals remain predominantly intact.

Similarly for samples with concentration below ϕ_g , prepared on the rotating wheel, the highly asymmetric and therefore thermodynamically unstable shear-induced structures dissipate by large-scale diffusion. However, for $\phi > \phi_g$, these structures remain frozen in the structurally arrested metastable fluid.

We now conjecture that infrequent small-scale collective motions, which occur as particles arrange themselves into registration on the shear-induced nuclei, provide a mechanism for the slow growth of the asymmetric crystals as well as the source of the small remnant decay observed in $f(q, \tau)$ at long times. To support this conjecture we show, in Figs. 6 and 7, intensity traces $I(t)$ with their corresponding time-averaged intensity autocorrelation functions $g_T^{(2)}(q, \tau)$ for two separate measurements on the same sample ($\phi = 0.581$). Recall that in the glass phase the fluid structure is arrested and only small-scale particle motions about a fixed amorphous distribution of average positions are possible. This behavior, expected for an ideal glass, is consistent with that indicated by the lower trace (b) in Fig. 6. Here the intensity versus time exhibits small fluctuations, associated with the local particle motions, on a constant component, associated with the fixed average positions. The corresponding intensity autocorrelation function [curve (b) in Fig. 7] decays to background [$(g_T^{(2)}(q, \tau) = 1)$] just beyond $10^5 \mu\text{sec}$. (The intensity fluctuations on time scale $\leq 10^5 \mu\text{sec}$ are disguised since the actual intensities are plotted only every 2 sec.) The large majority, of nearly 200 separate measurements made in different regions of this sample at the same angle, were similar to that just described. They showed the expected reduction in $g_T^{(2)}(q, 0)$ and variation in $\langle I(q) \rangle_T$ for measurements in different regions of the sample. However, for about 10% of the measurements the intensity trace showed, in addition to rapid fluctuations, much slower fluctuations or a steady drift in the mean intensity, as illustrated by the upper trace (a) in Fig. 6. The presence of these slow fluctuations is reflected in the intensity autocorrelation function, curve (a) in Fig. 7, which shows a slow long-time tail. This behavior for $\phi = 0.581$ is easily distinguished from that

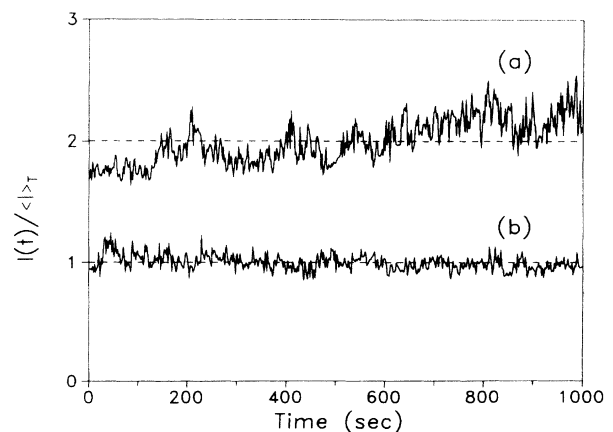


FIG. 6. Relative instantaneous intensity $I(t)/\langle I \rangle_T$ versus time, measured in different regions of the same colloidal glass ($\phi = 0.581$). The upper trace (a) has been raised by one unit.

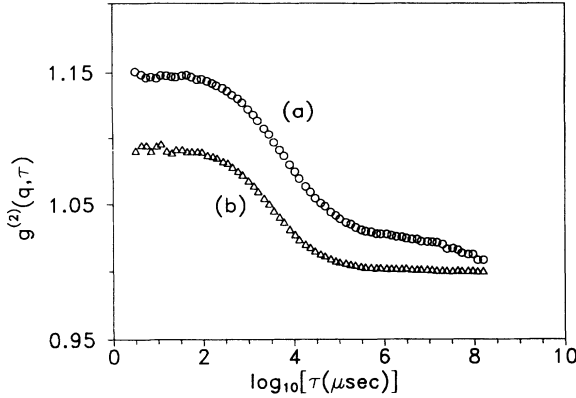


FIG. 7. Time-averaged intensity autocorrelation functions. Circles and triangles respectively correspond to the upper and lower intensity traces of Fig. 6.

for $\phi = 0.574$ ($< \phi_g$) where all intensity traces show both rapid and slow fluctuations but systematic drifts in $I(t)$ are never seen. These occasional slow and irregular variations in $I(t)$ for $\phi > \phi_g$ seem consistent with the occurrence of infrequent collective particle rearrangements that lead to the growth of large irregular crystals, discussed above. The results for $f(q, \tau)$, shown in Fig. 5, constitute an average over many individual measurements (see Table I).

As one goes deeper into the colloidal glass phase the large crystals no longer appear to be nucleated in the bulk of the sample but grow very slowly, over many days, from the meniscus and cuvette walls (see Fig. 1 in Ref. [12]). At these higher concentrations slow structural rearrangements are less frequent and, as shown in our earlier study of colloidal glasses [16], at long times $f(q, \tau)$ saturates to a value that remains constant over several decades. It appears that all particle motion and crystallization cease at the random-close-packing concentration $\phi = 0.64$.

Although large polydispersities can effect the form of $f(q, \tau)$, we suggest that for the suspensions studied here the polydispersity is sufficiently small ($\sim 4\%$) that its direct effect on the dynamics around the GT is insignificant. (However, there are other effects which we discuss in the following subsection.) Clearly, if a significant number of small mobile particles was present one would expect it to be uniformly distributed implying that all correlation functions, measured in all regions of the colloidal glass, should show a similar remnant decay at long times. It is interesting to contrast our suspensions of nearly monosized hard particles with the polydisperse suspensions of soft polystyrene particles used in similar studies by Bartsch *et al.* [47]. It is plausible that in the latter work the polydispersity (14–16%) may have been a significant factor contributing to the long-term restoration of ergodicity of the glass phase.

C. Comparison with mode-coupling theory

In the preceding subsections we located the GT concentration $\phi_g = \phi_c$ ($0.574 < \phi_c < 0.581$) as that where

both homogeneously nucleated crystallization and large-scale particle diffusion cease. We therefore identify ϕ_c with the critical concentration where the basic version of MCT predicts the ideal GT [7,8].

Although in principle the scaling time t_0 is the only quantity not specified by the theory for the hard-sphere system, in practice there are other quantities that cannot be stated exactly. In particular, due to the experimental uncertainty ($\sim 0.5\%$) in ϕ_c and ϕ , the physical separation parameter $(\phi - \phi_c)/\phi_c$ is approximate. However, the best MCT fits for the ISFs, obtained by using just t_0 and σ as free parameters, showed deviations of more than 10% [on a $\log_{10}(\tau)$ scale] from the experimental results. The critical volume fraction $\phi_c = 0.525$ predicted by MCT [26,27], for the hard-sphere system, differs from our experimental result by about 10%. Errors of this magnitude in ϕ_c , also expected in other quantities predicted by the theory [29,48], are possibly a consequence of errors in the approximations used for the static structure factor of the hard-sphere fluid in the metastable regime. The calculations of Fuchs *et al.* [29] give some indication of the sensitivity of $f_c(q)$ and ϕ_c to $S(q)$. Further to this, differences of 5–10% between the measured and predicted nonergodicity parameters for hard-sphere glasses were found in earlier work [16,42].

It appears therefore that at least one parameter in addition to the separation parameter and a scaling time is required to allow for the uncertainties in both the data and the numerical results of the theory. Thus, on the fluid side of the transition, $\phi < \phi_c$ ($\sigma < 0$), we attempt an analysis of the ISFs, shown in Fig. 5, in terms of a combination of the α and β processes in which we allow the time scale τ_α , the separation parameter σ , and the nonergodicity parameter $f_c(q)$ to vary. Because τ_α depends on both t_0 and σ , τ_α is used as a parameter in preference to t_0 . The fitting was performed as follows. First, the scaling time τ_α and amplitude $f_c(q)$ were estimated from the best fit of the ISF for the α process, given by Eq. (12), to the experimental ISF at long times. Second, the so-determined α process was then superposed with the β process, given by Eq. (11), with the master function $g'_-(\tau) = g_-(\tau) + B\tau^b$ for the β process alone. (The von Schweidler law [Eq. (14)] was subtracted from the function $g_-(\tau)$ to achieve this.) In this step σ was varied to obtain the best fit of the combined α and β processes to the data. Note that the time scale τ_β is fixed by σ and τ_α [Eq. (9)] and the critical amplitude $h(q)$ is determined by its ratio to $f_c(q)$, which is fixed by the theory. We emphasize that in performing these fits we comply with the constraints of MCT in that both $f_c(q)$ and $h(q)$ are independent of concentration and σ is independent of wave vector (see Sec. II). The scaling time τ_α was treated as the only unconstrained parameter and it therefore absorbs most of the random and systematic errors in the data.

It is evident from Fig. 5 (and Fig. 1 of Ref. [18]) that, beyond the influence of the microscopic transients ($\tau \gtrsim 10^4 \mu\text{sec}$), MCT fits to the data are possible over a matrix of wave vectors and suspension concentrations.

At $qR = 2.68$ [Fig. 5(a)] there are systematic

differences between the data and the optimum MCT fits. Here the amplitude $S(q)$ of the (unnormalized) coherent ISF, $F(q, \tau) = S(q)f(q, \tau)$ [see Eq. (20)], is roughly one-fiftieth of its peak value at $q = q_m$ and, as suggested in previous work [16,42], contributions from both incoherent scattering, associated with the small ($\sim 4\%$) spread in particle size, and multiple scattering may be expected. Multiple scattering may also contribute at larger wave vectors ($qR \gtrsim 4.1$) where the minimum of the single particle form factor is approached. In order to obtain the fits shown in Fig. 5(a) and Fig. 1(c) of Ref. [18] for $qR = 2.68$ and 4.10 , respectively, we required values for the ratio $h(q)/f_c(q)$, as shown in Fig. 8, which differ from those imposed by the theory by about 20%.

We now present several consistency checks for the parameters obtained in the above fitting process.

(i) The first and possibly the most significant consistency check is the fact that the ‘‘experimental’’ scaling times τ_α , seen in Fig. 9, show no systematic wave-vector dependence. This verifies the predicted α scale universality.

(ii) Figure 10 shows a comparison of the nonergodicity parameters $f_c(q)$ and critical amplitudes $h(q)$ required to obtain the above fits to the data, with the corresponding quantities predicted by MCT for the hard-sphere system [27]. Significantly, the values for the nonergodicity parameters obtained here are in agreement with direct measurements of this quantity [16,42].

In the colloidal glass, $\phi > \phi_c$, we assume that the α process is arrested and accordingly we analyzed the data in terms of the β process only. A detailed discussion is given elsewhere [16], but we include sufficient results here to contrast the behavior on either side of the GT. Due to statistical errors, possibly as a result of infrequent structural rearrangements associated with the slow growth of the large irregular crystals (discussed in Sec.

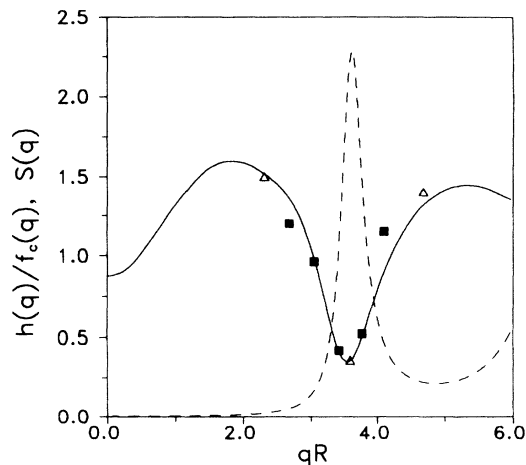


FIG. 8. Ratio $h(q)/f_c(q)$ of the critical amplitude to the nonergodicity parameter; the solid curve is the MCT result and the squares refer to the values obtained from the MCT fits to the data, shown in Fig. 5, for $\sigma < 0$ (open triangles apply to MCT fits to data for $\phi \leq 0.528$ and therefore warrant less significance than the squares). The dashed curve is the Percus-Yevick static structure factor for the hard-sphere fluid at $\phi = 0.575$ reduced in magnitude by a factor of 2.

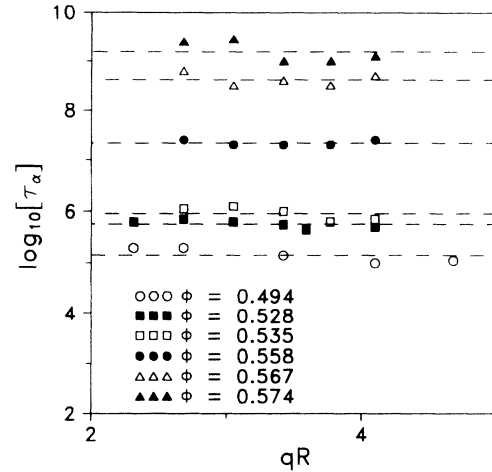


FIG. 9. Scaling times τ_α obtained from the best MCT fits to the data of Fig. 5. The dashed lines indicate average values.

IV B), small variations in $f_c(q)$ and $h(q)$ from those found for $\sigma < 0$ had to be tolerated to obtain the MCT fits to the data shown in Fig. 5. The resulting amplitudes are also shown in Fig. 10.

(iii) For $\sigma < 0$ the scaling times τ_β for the β process were calculated from Eq. (9) and for $\sigma > 0$ they were obtained directly from the fit of Eq. (11) to the experimental ISFs (see Ref. [16] for details). Equation (9) was also used to determine the microscopic transient time t_0 . The calculated times absorb not only the uncertainty in τ_α (or τ_β for $\sigma > 0$), but also the small variation (about 5%) in σ that could be tolerated without significant departure of the optimum MCT functions from the data. The three time scales are plotted as functions of the separation parameter in Fig. 11. For completeness and also to indicate consistency between different suspension preparations, results for τ_β from a previous study [16] are included. The

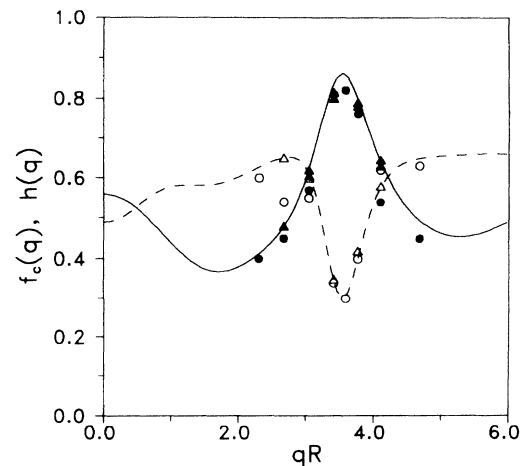


FIG. 10. Nonergodicity parameters $f_c(q)$ (closed symbols) and critical amplitudes $h(q)$ (open symbols). Circles refer to the fluid side ($\sigma < 0$) and triangles refer to the glass side ($\sigma > 0$) of the GT. The solid and dashed curves are the MCT predictions for $f_c(q)$ and $h(q)$, respectively, for the hard-sphere system.

theoretical curves for τ_α and τ_β [Eq. (9)] are calculated with the average value $t_0 = 10^3 \mu\text{sec}$ for the microscopic transient time. Thus the comparison between experiment and theory, shown in Fig. 11, involves no further adjustable parameters and the agreement therefore represents another consistency check of MCT.

The uncertainties in t_0 are such that a weak concentration dependence, as a consequence of hydrodynamic interactions, is not precluded. Also, there is no rigorous criterion for the range of validity of the asymptotic MCT predictions used in these analyses; the concentration $\phi = 0.494$, for which we obtain the separation parameter $\sigma = 0.2$, is probably too far from the critical point for this analysis to be applicable.

Note that the times τ_α and τ_β show the predicted divergence and separation as σ approaches zero from below; for $\sigma = -0.1$, $\tau_\alpha/\tau_\beta \sim 8$, while for $\sigma = -0.0035$, the smallest negative separation from the GT used in this work $\tau_\alpha/\tau_\beta \sim 180$. In addition, the concentration dependence of the crossover time τ_β is consistent with the predicted symmetry about the GT. We point out, however, that τ_β should not be interpreted as a characteristic time associated with a particular physical relaxation process. Indeed such interpretation is precluded on the basis of the fractal decay indicated by the power law predicted for the early part of the β process. It follows from Eqs. (9), (11), and (13) that this stage of the relaxation can be written as

$$f(q, \tau) = f_c(q) + h(q)(\tau/t_0)^{-a}. \quad (24)$$

According to MCT τ_β represents the *crossover* from the β to the α process; the latter describes structural relaxation towards equilibrium, characterized by the time scale τ_α . Below ϕ_c structural relaxation slows with increasing ϕ so that τ_α and also τ_β increase. In the glass phase the α pro-

cess is arrested and here τ_β marks the crossover from the above ϕ -independent power law to the plateau

$$f(q, \infty) = f_c(q) + |\sigma|^{1/2} h(q)(1-\lambda)^{-1/2}. \quad (25)$$

Thus the reduction in τ_β with increasing ϕ (or σ) is a consequence of the concomitant increase in the asymptote $f(q, \infty)$.

(iv) A fourth and final consistency check of the theory is contained in a plot of the separation parameter versus volume fraction shown in Fig. 12. A linear least-squares fit to these results [see Eq. (8)] which excludes the point at the lowest concentration (for reasons mentioned above) gives $\phi_c = 0.571 (\pm 0.003)$ for the critical concentration and $c_0 = 1.27$ for the constant that connects the theoretical and physical separations [Eq. (8)]. The latter result is consistent with that ($1.2 < c_0 < 1.4$) estimated by MCT for the hard-sphere system [29].

The ability to fit the MCT functions, given by Eqs. (11) and (12), to the experimental data immediately verifies the factorization property of the β process and the superposition principle of the α process. However, it is interesting and instructive to explicitly demonstrate these features.

The times τ_α can be used for a conventional test of the superposition principle of the α process by plotting the ISFs in terms of the rescaled time τ/τ_α , shown in Fig. 13 (and for two additional wave vectors in Fig. 4 of Ref. [18]). Where the ISF's are consistent with this principle, approximately from τ_β [for $\phi = 0.574$, $\log_{10}(\tau_\beta/\tau_\alpha) \sim -2$] they also follow the master functions [given by Eq. (12)] for the α process. However, one also sees from Fig. 13 that for times less than τ_β a significant fraction, equal to $1 - f_c(q)$, of the ISFs does not scale.

According to MCT the dynamics between the time scale of the microscopic motions and that of the α process is governed by the β process. This interval lies approximately between $10^4 \mu\text{sec}$ and τ_β , indicated by the two inflection points in $f(q, \tau)$ versus $\log_{10}(\tau)$ (seen in Fig. 5). The results in Fig. 14 are therefore crucial in that

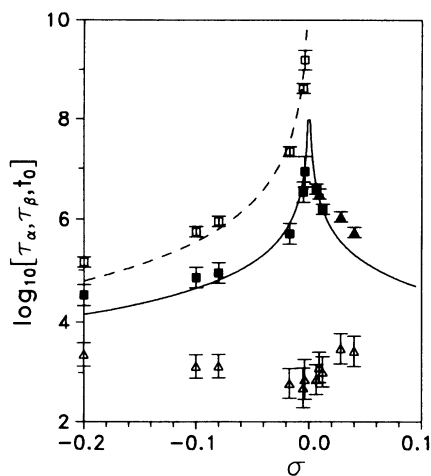


FIG. 11. Scaling times τ_α (open squares) and τ_β (closed squares) versus the separation parameter σ , obtained from MCT fits to the data. See Sec. IV C for further details. Results for τ_β from Ref. [16] are shown by the closed triangles. The microscopic times t_0 are indicated by the open triangles. The dashed and solid curves represent MCT predictions for τ_α and τ_β , respectively.

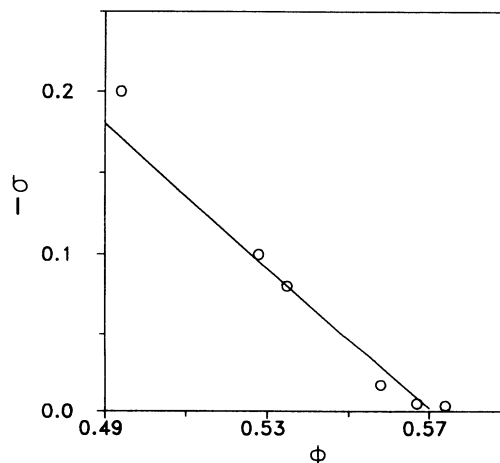


FIG. 12. Separation parameter σ versus volume fraction ϕ . The line is the result of a linear regression. See text for further details.

they demonstrate the factorization property of the β process for this time interval, i.e., where the quantity $[f(q, \tau) - f_c(q)]/h(q)$ [see Eq. (11)] is independent of q . As expected, τ_β and the temporal range over which the factorization property is satisfied decrease when the concentration is reduced and recedes from the GT [compare

Figs. 14(a) and 14(b)]. In the time window where the factorization property is obeyed the functions $[f(q, \tau) - f_c(q)]/h(q)$ trace the master function $|\sigma|^{1/2}g_{\pm}(\tau/\tau_\beta)$ of the β process.

Master functions for other values $\lambda=0.70$ and 0.80 of the exponent parameter were fitted to the data over the

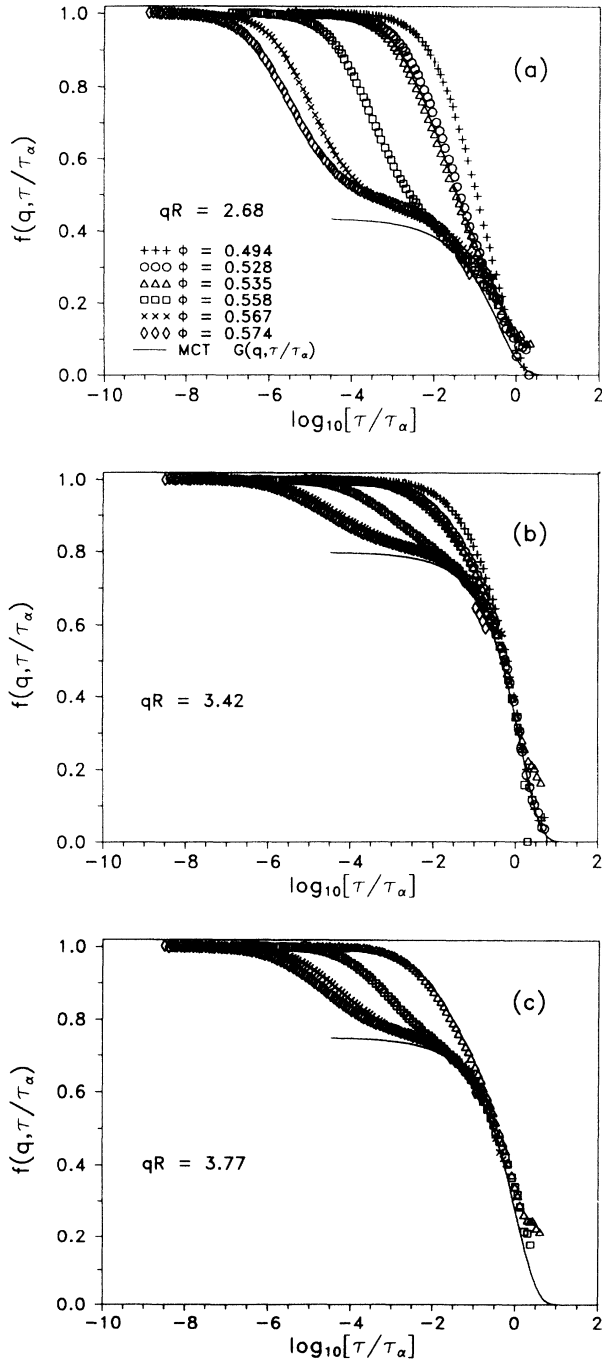


FIG. 13. Intermediate scattering functions, at the three wave vectors qR indicated in (a)–(c) as functions of the rescaled time τ/τ_α . The symbols refer to the volume fractions indicated in (a). The solid curves represent the functions [Eq. (12)] for the α process with the amplitudes $f_c(q)$ shown in Fig. 10 and master functions $G(q, \tau/\tau_\alpha)$ shown in Fig. 2.

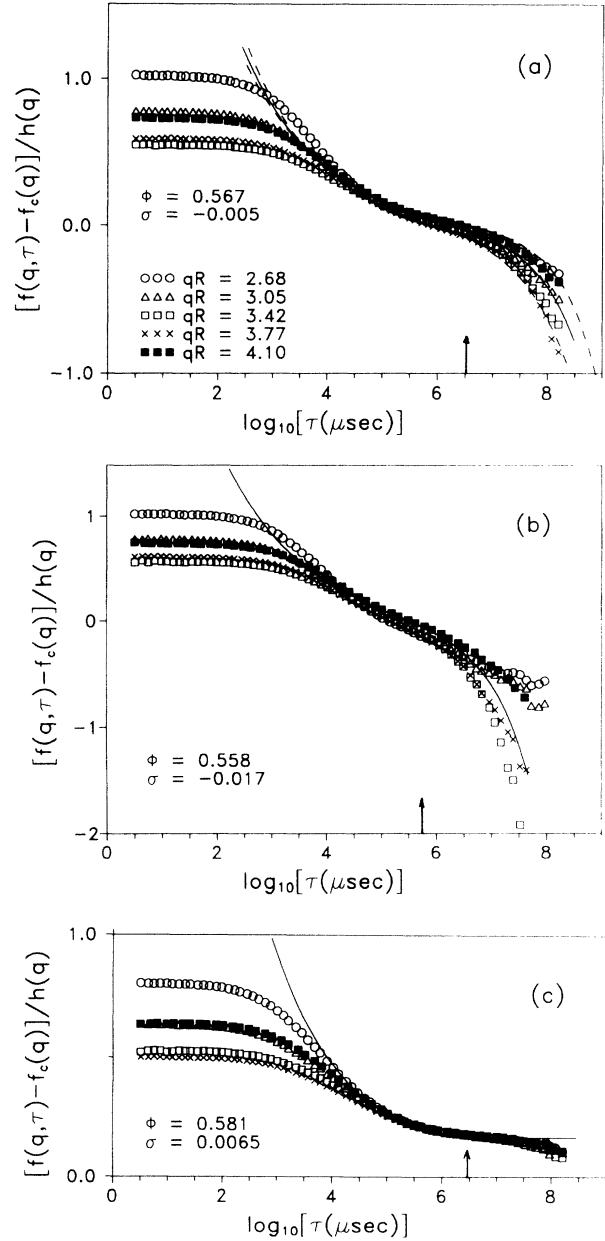


FIG. 14. Intermediate scattering functions scaled according to Eq. (11). Thus $[f(q, \tau) - f_c(q)]/h(q)$ is plotted as a function of the logarithm of delay time. The symbols represent the experimental data at the wave vectors indicated in (a). (a) and (b) are for suspensions on the fluid side of the GT at the separation parameters indicated. (c) is for the suspension just above the GT. The solid curves are the quantities $|\sigma|^{1/2}g_{\pm}(\tau/\tau_\beta)$ for $\lambda=0.758$ and scaling times τ_β and separation parameters σ shown in Figs. 11 and 12. The same quantities are shown as dashed curves in (a) for $\lambda=0.70$ and 0.80 (see text for further explanation). The vertical arrows indicate τ_β .

above-mentioned time window by varying σ . The results of this procedure, shown in Fig. 14(a), indicate that a 5% variation of the exponent parameter about the value $\lambda=0.758$ predicted for the hard-sphere system [27] is the most that can be tolerated.

At times beyond τ_β systematic deviations from the master function of the β process, seen in Figs. 14(a) and 14(b), must then be attributed to the α process. These deviations, being negative for wave vectors ($qR=3.42$ and 3.77) near the position of the peak in $S(q)$ and positive for the other wave vectors, are consistent with the wave-vector dependence of the first correction to the von Schweidler decay due to the α process [28].

A comprehensive verification of the factorization property of the β process for colloidal glasses is contained in a previous paper [16]. However, again for completeness, we include an illustration of this property [Fig. 14(c)] for the lowest concentration colloidal glass ($\phi=0.581$ and $\sigma=0.0065$).

The implication of the above discussion is that the structural dynamics, beyond the microscopic transients, in very concentrated metastable fluids cannot be described by a process centered on a single characteristic time, such as the stretched exponential function. In fact, Bartsch *et al.* [47] have already shown that relaxation data obtained for a system similar to ours cannot be satisfactorily explained even with a sum of two stretched exponentials. However, the master functions $G(q, \tau)$ of the α process (shown in Fig. 2) can be approximated by the stretched exponential [28], i.e., for $\tau \gg \tau_\beta$ Eq. (12) can be expressed by

$$f(q, \tau) = f_c(q) \exp[-(\tau/\tau_e)^\beta]. \quad (26)$$

MCT predicts that both the time scale τ_e and the stretching parameter β are functions of the wave vector. Our results in Fig. 13 are consistent with these predictions in that τ_e varies with wave vector by almost one decade as the position of the structure factor peak is traversed. Unfortunately, the noise in the data precludes conclusive comment regarding the predicted subtle q dependence of β [28].

V. CONCLUSIONS

Suspensions of nearly identical hard spherical particles, used in this and previous work, appear to constitute the simplest experimental systems to show a glass transition. As far as experimental uncertainties in the definition of concentration permit, a kinetic GT is located at the same concentration where homogeneous crystallization is suppressed. Although crystallization by homogeneous nucleation does not occur beyond the GT concentration, slow crystal growth still proceeds. Figures 6 and 7 provide further evidence consistent with our conjecture that, in the colloidal glass, crystal growth occurs through small-scale collective particle rearrangements on irregularly distributed shear-induced nuclei. Despite this apparent gradual restoration of ergodicity in colloidal glasses, the simplicity of the interparticle interactions and the absence of hopping motions suggest that sterically stabilized colloidal suspensions provide a valuable refer-

ence system for conventional, but invariably more complex, glass formers and also for assessing the basic version of MCT.

In the first DLS studies [14] of metastable colloidal fluids and glasses the measured ISFs spanned a time window of up to five decades. The ISFs measured at the position of the primary structure factor peak q_m were analyzed quite successfully in terms of the β process only [15]. Due to the large amplitude $f_c(q_m)$ of the α process that pertains at q_m and the limited dynamic window, this analysis was not unique and the ISFs beyond the microscopic processes could also be fitted to a stretched exponential [29].

In the present work the GT is traversed in smaller concentration increments. This, combined with the accumulation of relaxation data spanning an eight decade time window and a significant range of wave vectors, allows us to make significantly more specific comments on the predictions of MCT.

Our analysis shows that on the fluid side of the GT and beyond the time of the microscopic transients, the ISFs can be quantitatively described by the superposition of the α and β processes; close to the transition the predicted functions follow the data over a time frame of nearly five decades. This immediately verifies the scaling property of the α process and the factorization property of the β process. In particular the factorization of correlations in space and time, the essential signature of the β process, is verified for a dynamic range of about three decades close to the GT. Systematic departures from factorization at long times signal the onset of a different process. At these long times the ISFs can be scaled in time so that they follow the master functions of the α process. However, only a (wave-vector-dependent) fraction of the ISFs obeys this superposition principle. These findings lead to the conclusion that neither the α process alone nor the β process alone can account for the slow structural relaxation in metastable colloidal fluids as they near the GT. Once the GT is crossed, the ISFs settle to a constant value at long times signaling the arrest of the α process. Furthermore, the consistency checks contained in Figs. 7–12 allow us to make the following summary of our results in terms of MCT: All our measured ISFs outside the microscopic transients can be described by the basic version of MCT to an accuracy of about 10% in the neighborhood of q_m , where coherent scattering is strong, and to an accuracy of about 20% away from q_m , where coherent scattering is weak, using a single fit parameter t_0 . The error margins reflect to some extent our experimental uncertainties but also systematic errors of the theory. This description extends over four to five decades in time, holds for a significant spread in wave vectors, and for relaxation times that vary over five decades for the eight concentrations analyzed.

ACKNOWLEDGMENTS

We are grateful to M. Fuchs for providing tabulations of the α process master functions. We also thank M. Fuchs, W. Götze, and R. O'Sullivan for valuable discussions and P. Francis for his technical assistance. This work was supported by the Australian Research Council.

- [1] J. Jäckle, *Rep. Proc. Phys.* **49**, 171 (1986).
- [2] G. H. Fredrickson, *Annu. Rev. Phys. Chem.* **39**, 149 (1988).
- [3] C. A. Angell, *J. Phys. Chem. Solids* **49**, 863 (1988).
- [4] J. P. Sethna, J. D. Shore, and M. Huang, *Phys. Rev. B* **44**, 4943 (1992).
- [5] *Slow Dynamics in Condensed Matter*, edited by K. Kawasaki, M. Tokuyama, and T. Kawakatsu, AIP Conf. Proc. 256 (AIP, New York, 1992).
- [6] J. Jäckle, *J. Phys.: Condens. Matter* **1**, 267 (1989).
- [7] W. Götze, in *Liquids, Freezing and the Glass Transition*, edited by J. P. Hansen, D. Levesque, and J. Zinn-Justin (North-Holland, Amsterdam, 1991), p. 287.
- [8] W. Götze and L. Sjögren, *Rep. Prog. Phys.* **55**, 241 (1992).
- [9] C. A. Angell *et al.*, in *Slow Dynamics in Condensed Matter* (Ref. [5]), p. 3.
- [10] J. Ullo and S. Yip, *Phys. Rev. A* **39**, 5877 (1989).
- [11] D. Thirumalai and R. D. Mountain, *Phys. Rev. E* **47**, 479 (1993).
- [12] P. N. Pusey and W. van Megen, *Nature (London)* **320**, 340 (1986).
- [13] P. N. Pusey and W. van Megen, *Phys. Rev. Lett.* **59**, 2083 (1987).
- [14] W. van Megen and P. N. Pusey, *Phys. Rev. A* **43**, 5429 (1991).
- [15] W. Götze and L. Sjögren, *Phys. Rev. A* **43**, 5442 (1991).
- [16] W. van Megen and S. M. Underwood, *Phys. Rev. E* **47**, 248 (1993).
- [17] C. G. de Kruif, E. M. F. van Iersel, A. Vrij, and W. B. Russel, *J. Chem. Phys.* **83**, 4717 (1985); G. N. Choi and I. M. Krieger, *J. Colloid Interface Sci.* **113**, 101 (1986); L. Marshall and C. F. Zukoski, *J. Phys. Chem.* **94**, 1164 (1990); D. A. R. Jones, B. Leary, and D. V. Boger, *J. Colloid Interface Sci.* **147**, 479 (1991).
- [18] W. van Megen and S. M. Underwood, *Phys. Rev. Lett.* **70**, 2766 (1993).
- [19] B. J. Ackerson, *J. Chem. Phys.* **69**, 684 (1978).
- [20] B. Cichocki and W. Hess, *Physica A* **141**, 475 (1987).
- [21] G. Szamel and H. Löwen, *Phys. Rev. A* **44**, 8215 (1991).
- [22] K. Kawasaki, *Phys. Rev.* **150**, 291 (1966); *Ann. Phys. (N.Y.)* **61**, 1 (1970).
- [23] P. N. Pusey and R. J. A. Tough, in *Dynamic Light Scattering*, edited by R. Pecora (Plenum, New York, 1985).
- [24] G. Li, W. M. Du, X. K. Xen, H. Z. Cummins, and N. J. Tao, *Phys. Rev. A* **45**, 3867 (1992); G. Li, W. M. Du, A. Sakai, and H. Z. Cummins, *ibid.* **46**, 3343 (1992).
- [25] L. Verlet and J. J. Weis, *Phys. Rev. A* **5**, 939 (1972).
- [26] U. Bengtzelius, W. Götze, and A. Sjölander, *J. Phys. C* **17**, 5915 (1984).
- [27] J. L. Barrat, W. Götze, and A. Latz, *J. Phys.: Condens. Matter* **1**, 7163 (1989).
- [28] M. Fuchs, I. Hofacker, and A. Latz, *Phys. Rev. A* **45**, 898 (1992).
- [29] M. Fuchs, W. Götze, S. Hildebrand, and A. Latz, *Z. Phys. B* **87**, 43 (1992).
- [30] M. Fuchs, W. Götze, S. Hildebrand, and A. Latz, *J. Phys.: Condens. Matter* **4**, 7709 (1992).
- [31] H. Z. Cummins, W. M. Du, M. Fuchs, W. Götze, S. Hildebrand, A. Latz, G. Li, and N. J. Tao, *Phys. Rev. A* **47**, 4223 (1993).
- [32] P. N. Pusey and W. van Megen, *J. Chem. Phys.* **80**, 3513 (1984).
- [33] S. E. Paulin and B. J. Ackerson, *Phys. Rev. Lett.* **64**, 2663 (1990).
- [34] W. van Megen, P. N. Pusey, and P. Bartlett, *Phase Transitions* **21**, 207 (1990).
- [35] W. G. Hoover and F. H. Ree, *J. Chem. Phys.* **49**, 3609 (1968).
- [36] J. D. Weeks, *Phys. Rev. B* **24**, 1530 (1981).
- [37] W. van Megen and S. M. Underwood, *Nature (London)* **362**, 616 (1993).
- [38] P. N. Pusey and W. van Megen, in *Physics of Complex and Supermolecular Fluids*, edited by S. A. Safran and N. A. Clark (Wiley, New York, 1987).
- [39] B. J. Berne and R. Pecora, *Dynamic Light Scattering* (Wiley, New York, 1976).
- [40] P. N. Pusey, in *Photon Correlation Spectroscopy and Velocimetry*, edited by H. Z. Cummins and E. R. Pike (Plenum, New York, 1977).
- [41] P. N. Pusey and W. van Megen, *Physica A* **157**, 705 (1989).
- [42] W. van Megen, S. M. Underwood, and P. N. Pusey, *Phys. Rev. Lett.* **67**, 1586 (1991).
- [43] J. G. H. Joosten, E. T. F. Gelade, and P. N. Pusey, *Phys. Rev. A* **42**, 2161 (1990).
- [44] W. van Megen and P. N. Pusey (unpublished).
- [45] W. van Megen, R. H. Ottewill, S. M. Owens, and P. N. Pusey, *J. Chem. Phys.* **82**, 508 (1985).
- [46] B. J. Ackerson, *J. Rheol.* **43**, 553 (1990).
- [47] E. Bartsch, M. Antonietti, W. Schupp, and H. Sillescu, *J. Chem. Phys.* **97**, 3950 (1992); E. Bartsch, V. Frens, S. Moller, and H. Sillescu, *Physica A* **201**, 363 (1993).
- [48] M. Fuchs (private communication).